ISSN 1063-7826, Semiconductors, 2018, Vol. 52, No. 7, pp. 907–913. © Pleiades Publishing, Ltd., 2018.
Original Russian Text © I.P. Ivanenko, S.V. Krasnoshchekov, A.V. Pavlikov, 2018, published in Fizika i Tekhnika Poluprovodnikov, 2018, Vol. 52, No. 7, pp. 768–774.

CARBON SYSTEMS

Analysis of the Structure and Conductivity of Kinked Carbon Chains Obtained by Pulsed Plasma Deposition on Various Metal Substrates

I. P. Ivanenko[a]*, S. V. Krasnoshchekov[b], and A. V. Pavlikov[a]

[a] *Moscow State University, Faculty of Physics, Moscow, 119991 Russia*

[b] *Moscow State University, Faculty of Chemistry, Moscow, 119991 Russia*

**e-mail: ivanenko@physics.msu.ru*

Submitted June 8, 2017; accepted for publication June 19, 2017

Abstract—Linear-chain carbon films with a thickness of order 100 nm were studied by tunneling spectroscopy. The oscillating dependence of the differential conductivity of the investigated structures is established. The results obtained are interpreted using a model of charge-density wave formation in regular structural kinks of carbon chains. The Raman spectra of the films are recorded. The simulated spectra of harmonic oscillations of polyines $(-C{\equiv}C-)_n$ and cumulenes $(=C=)_n$ of carbon films are theoretically compared.

DOI: 10.1134/S1063782618070102

1. INTRODUCTION

One of the most promising forms of carbon materials is linear–chain carbon (LCC) [1]. In this work, we investigate carbon films formed by low-temperature pulsed plasma-ion-assisted deposition [2]. LCC consists of chains of carbon atoms oriented perpendicularly to the substrate surface. The structure and electrical properties of these films were previously investigated in [3–5]. In recent years, there has been increased interest in LCC films [5].

The aim of this study is to investigate the transport properties of LCC using tunneling spectroscopy (TS), analyze the molecular structure by comparing the experimental and calculated Raman spectra, and examine the correlation between the properties of the substrate material and deposited structure. We study the dependence of the transport properties of condensed LCC films on substrates made of different metals. The chosen substrate metals are Cu, Mo, W, and Al. The average thickness of the condensed films on the substrate is about 100 nm.

Tunneling microscopy study of the transport processes occurring in metallic substrate–LCC heterostructures provides information about their electrical properties, which is confirmed by other investigations [6–11]. This technique is based on the phenomenon of electron tunneling through a potential barrier between a metallic probe consisting of Pt and Ir alloy and the sample surface in an applied electric field. The tunnel current is mainly determined by the barrier transmittance (distance to the surface and applied voltage). In addition, the tunnel current is affected by the shape of the density of states both on the microscope tip and in the film, as well as the electron mobility in the film conduction layer [12, 13].

2. EXPERIMENTAL

The conductivity of the obtained heterostructures was studied using a FemtoScan microscope [14] in the tunneling spectroscopy mode. The I–V characteristics were measured at a fixed probe position at one point above the sample surface. The differential conductivities of the structures were calculated. Figure 1 shows a typical differential I–V characteristic of the films.

The tunneling current density can be described by the Simmons formula [12]. To interpret the experimental data, it is difficult to use the general formula. Therefore, one of three approximations was used [12, 13]. The conditions of our experiment correspond to the case when the applied voltage is comparable with the surface work function.

The effects of room-temperature differential conductivity oscillations have features caused by the specific structure of carbon. For all the metallic substrates used in the experiment, we observed differential conductivity oscillations with approximately the same period for each structure, which was calculated by averaging all of the peaks. The oscillation period is several times larger than the heat energy at 300 K. Such differential conductivity oscillations in carbon and semiconductor structures were observed previously in [6–9].

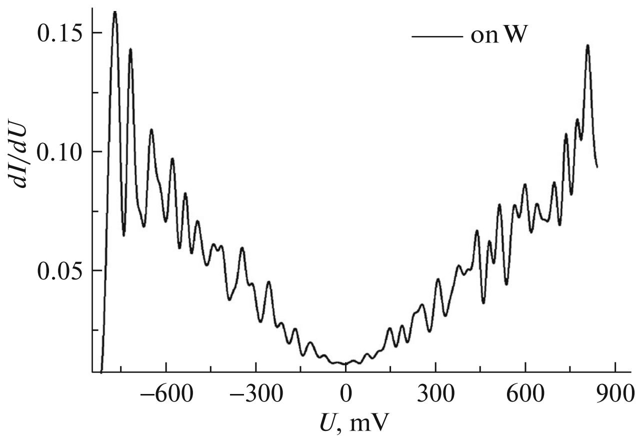

Fig. 1. Typical plot of tunneling conductivity oscillations for the film deposited on tungsten.

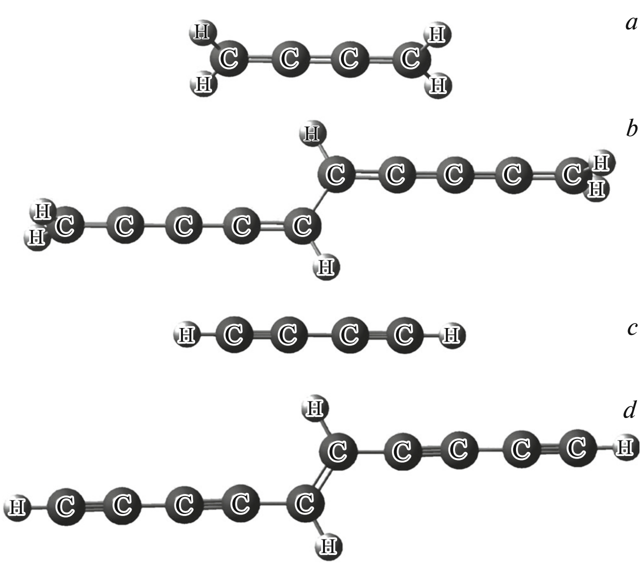

Fig. 2. Calculated models: (*a*) single cumulene consisting of four carbon atoms, (*b*) double cumulene consisting of ten carbon atoms, (*c*) single polyine consisting of four carbon atoms, and (*d*) double polyine consisting of ten carbon atoms. The use of a single chain means the use of a single linear chain of carbon atoms and the use of a double chain means the occurrence of a kink between linear components.

We assumed one-dimensional charge density waves (CDWs) to be formed along the carbon chain. The standing wave period in LCC should correlate with the linear fragment length with the formation of a superstructure. Obviously, the amplitude of the electrical-conductivity wave function at the chain kink should be zero. For the Cu, W, Mo, and Al substrates, we obtained average numbers of carbon atoms n of 28, 22, 18, and 12 in the chain, respectively, using the formula

$$n = \left(\frac{12.25}{2\sqrt{E}}\right)/1.3. \qquad (1)$$

The mean distance between carbon atoms in a chain was assumed to be 0.130 nm and the wavelength was calculated basing on the de Broglie wave. Previously, Chalifoux et al. [15] obtained molecules with 44 carbon atoms [15].

3. CALCULATION TECHNIQUE

To identify the types of carbon bonds in the synthesized structure, we used Raman spectroscopy and simulation (Fig. 2). As we show below, a model without kinks does not explain the Raman spectra. The harmonic oscillations of molecules consisting of carbon chains of the cumulene $(=C=)_n$ and polyine $(-C\equiv C-)_n$ types were calculated using their basic structure without kinks or with the only kink between linear fragments. The terminal groups were simulated by hydrogen atoms basing on the data reported in [16–19].

Optimization of the geometric structures and calculation of the matrix of second derivatives of the electron energy and components of the electrooptical properties were performed using the Gaussian 9.0 program package [20]. The further calculation of normal oscillations and simulation of the Raman spectra were performed using the ANCO program in accordance with the investigations carried out in [21–24].

The optimized geometric structures and harmonic force fields were calculated using the quantum-mechanical second-order Möller–Plesset (MP2) technique with the aug-cc-pVTZ basis set. The adequacy of the model was demonstrated in [25].

To study the effect of a number of carbon atoms on the predicted oscillatory modes, we chose the following set of molecules: (ps) single polyines (4, 6, and 8 carbon atoms), (pd) double polyine (with a kink) (3 and 5 atoms in a molecule), (cs) single cumulene (3, 5, and 6 carbon atoms), and (cd) double cumulene (4 and 5 atoms). The calculated spectra for all molecule types are presented in Fig. 3.

The size and complexity of the investigated molecules, the diversity of their structures, and the presence of a carbide bond with the substrate (Cu, Mo, W, and Al) yield fairly complex experimental spectra.

Figure 4 shows the experimental Raman spectra. To detect the Raman spectra, we used a Horiba Jobin Yvon HR800 micro-Raman spectrometer. The Raman spectra were excited by a laser with a wavelength of 633 nm. It can be easily seen that the best agreement between the theory and experiment is obtained for the long-chain (pd) and (cd) types.

Indeed, the experimental Raman spectrum contains a broad band with a peak intensity maximum of ~1600 cm^{-1}, which corresponds to the double bond

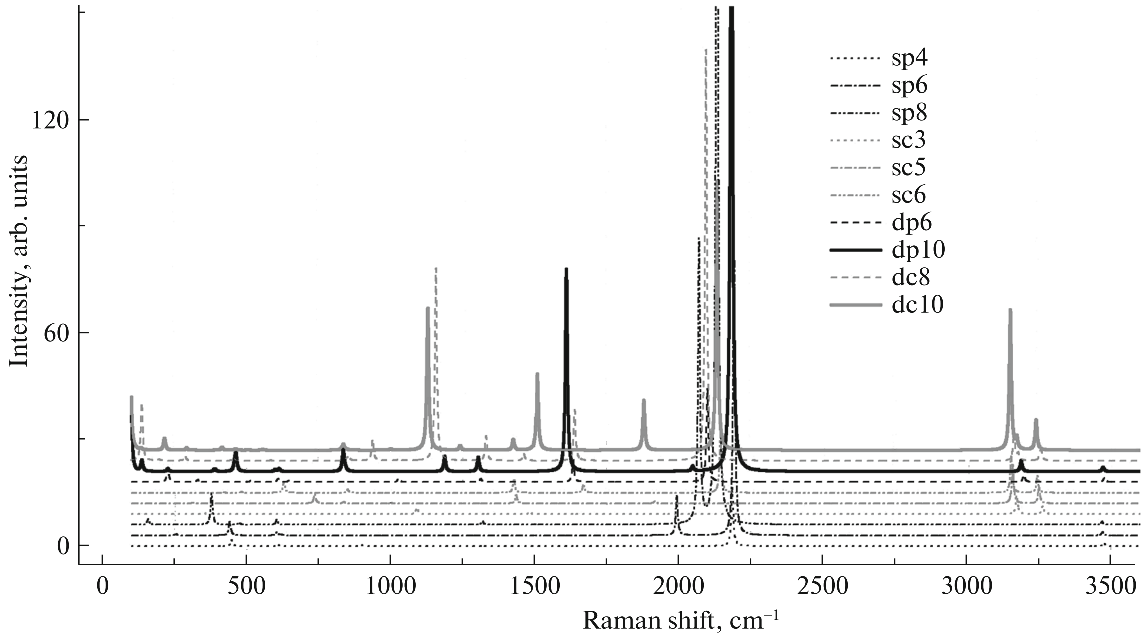

Fig. 3. Calculated Raman scattering spectra of molecules for (sp) single polyine, (sc) single cumulene, (dp) double polyine, and (dc) double cumulene. The numbers of carbon atoms in the structure are given.

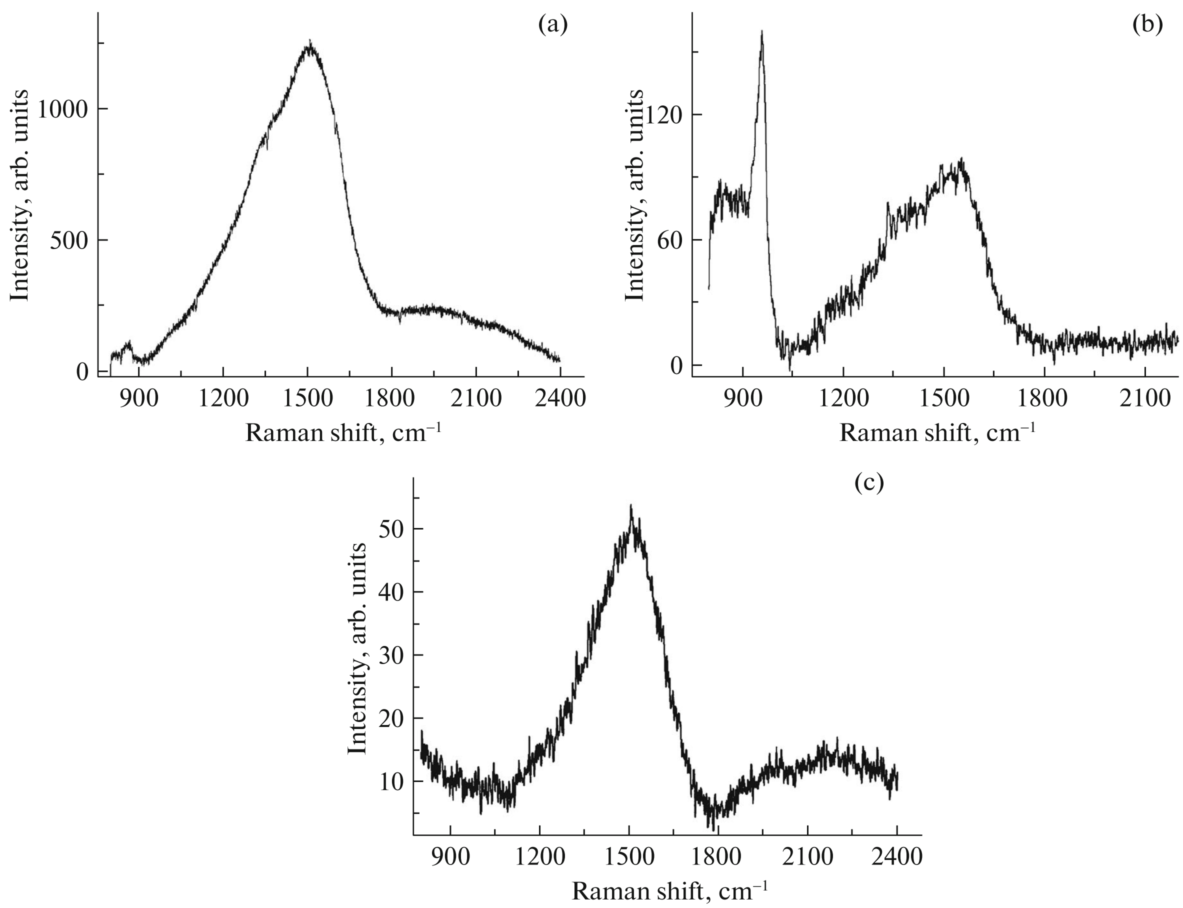

Fig. 4. Experimental Raman spectra of the films on (a) Al, (b) Mo, and (c) W substrates. Deposition was performed on all the substrates simultaneously.

oscillation frequency at the kink between the linear fragments of the chain (the so-called *G* peak) [26, 27].

The calculations show that the bands in the range of 1000–1700 cm^{-1} are indicative of the presence of molecules belonging to structures with kinks between chains (cd8, cd10, pd6, and pd10), which was not observed in the models without a kink in earlier study [27]. In addition, a low-frequency (400–980 cm^{-1}) region arises, which was not described in publications [5]. The oscillations of carbon atoms, which propagate parallel to the substrate (beyond the plane), belong to the low-frequency region.

The oscillation frequencies related to the chain kink in the pd10 model are 1304 and 1229 cm^{-1}, which corresponds to δ(C=C–H) def. and 1609 cm^{-1} to ν(C=C) for the kink; in the pd6 model, 1313 and 1282 cm^{-1} responsible for δ(C=C–H) def. and 1634 cm^{-1} to ν(C=C) for the kink; in the dc8 model, 1158 cm^{-1} to δ(C=C–H) def. and ν(C=C) for the kink, 1332 cm^{-1} to δ(C=C–H) def. and ν(C=C) str. near the kink, 1639 cm^{-1} δ(C=C–H) def., ν(C=C) str., and δ(C=C–H) def. at the end of the chain; in the dc10 model, 1128, 1241, and 1509 cm^{-1} δ(C=C–H) def. and ν(C=C) str. near the kink, 1425 cm^{-1} δ(C=C–H) def. with δ(C=C–H) def. at the end of the chain. The features in the spectral range of 1300–1600 cm^{-1} are related to the presence of sp^2 bonds [28].

It can be seen from Table 1 that the bands at 1129 and 1158 cm^{-1} are related to C–C bond oscillations and belong to the pd10 and pd8 structures, respectively. They are similar to the bands at 1140 and 1470 cm^{-1}, which is typical of diamond nanocrystals smaller than 2 nm [29]. The bands with frequencies of 1609 and 1634 cm^{-1} are related to oscillations of double C=C bonds and belong to cd10 and cd6 structures.

A single C–C bond is characterized by frequencies near 1188 cm^{-1} for the pd10 model and 1319 cm^{-1} (this maximum is often referred to as the *D* peak for the ps8 model). The position of this band is similar to a frequency of 1330 cm^{-1}, which corresponds to a “normal” diamond with fairly large crystallites [28]. The double C=C bond is characterized by frequencies of 2132 and 1879 cm^{-1} for the cd10 model. For the cd8 model, these frequencies are shifted to 2095 and 1639 cm^{-1}. In a linear molecule, the bands of the same bond have lower intensity and their positions correspond to frequencies of 2145 and 1670 cm^{-1} for the cs6 model, while the frequencies for the cs5 model are 2187 and 1916 cm^{-1} and the frequency for the pd10 model is 1609 cm^{-1}. The C=C bond is characterized by frequencies of 2182 and 2047 cm^{-1} for the pd10 model and a decrease in the molecule size to 6 atoms (the pd6 model) yields frequencies of 2100 and 1634 cm^{-1}, respectively. In a linear molecule, the corresponding mode has a low-intensity peak at 2186 cm^{-1}. The band between 1800 and 2200 cm^{-1} (the so-called *C* band) is related to the modes of expansion of *sp*-hybridized carbon. The *C* band contains the main peak near 2100 cm^{-1} *C*2 and a shoulder with a lower peak of the frequency *C*1 near 1980 cm^{-1} [30].

The spectral region with characteristic oscillations of triple C≡C bonds also contains frequencies for single bonds: 2133 and 2070 cm^{-1} in the ps8 model. An analogous situation is observed in the frequency band of the C–C bond, which coincides with the frequencies for the C–C–H kink on chain kinks, creating a frequency of 1157 cm^{-1}.

The experimental spectra were decomposed into components described by the Gaussian form, as was proposed in [31–33]. Comparing the simulated spectra with the spectra of the films formed on different substrates, we can conclude that the film on Cu apparently belongs to the pd10 model, which is consistent with the results of [34] with inclusions of the cs3 and pd6 models; the film on Mo belongs to the cd8 model with small pd10 and cd10 fractions; the film on W belongs to the cd10 model with the cd8 inclusion; and the film on Al corresponds to the cd10 structure with pd6, cs6, and cd8 inclusions. This can be related to impurities in metals. The film synthesis technique used includes ion bombardment of the substrate with subsequent sputtering of the substrate metal and possible diffusion of the latter along the chain. Thus, we can assume that the substrate atoms can serve as impurities related to the LCC kinks.

The spectra of all films have a maximum with a frequency of 1050 cm^{-1}, which is referred to as a *T* peak [35]; but, it was only detected upon UV excitation. We can observe a band with a frequency of ~1470 cm^{-1}, which was described in publications as characteristic of only films consisting of carbon spheres [36] or as an expansion mode for CC transpolymer with frequencies of 1078 and 1458 cm^{-1} [37]. Amorphous carbon is characterized by a broad band with a center at 1480 cm^{-1} [38]. The three maxima, 996, 1116, and 1498 cm^{-1}, also arise in the amorphous carbon spectrum or can be attributed to the cumulene carbine structure stabilized by disperse Cu atoms from the substrate [39] and the bands near 2150 cm^{-1} are related to the polyine structure of carbines [40, 41]. The band with a frequency of 1250 cm^{-1} was found in graphene-type carbon [42]. The changes in the diagrams of the Raman spectra of amorphous carbon presented in study [28] are very useful. The broad form of the Raman scattering bands can be caused by a random shift of the next link in a long chain.

In addition, we calculated the LCC kink angles for dc8, dc10, and dc12 and obtained 122.00, 122.190, and 122.720 and 122.560 and 122.480 for dp6 and dp10, which is consistent with the data from [17]. The difference consists in the model of the chain with regard to BLA.

Table 1. Experimental oscillation frequencies in the Raman spectra for extracting Cu, Mo, W, and Al substrates based on harmonic analysis

Experiment: substrate, wavenumber, and intensity*				Designation**	Calculated frequency: molecule type, frequency (cm^{-1}), intensity (Å/a.m.u.), and fundamental frequency (ν_i)
Cu	Mo	W	Al		
	2140m	2171w	2226vw	ν(C≡C) str., ν(C=C) str.	dc10: ν_2 = 2132(3470); sc5: ν_7 = 2187(3) sc6: ν_2 = 2145(783); dp10: ν_2 = 2182(10698); sp8: ν_2 = 2133(12992); sp6: ν_2 = 2192(3942); sp4: ν_2 = 2186(792).
2070s	2011vw	2002m	2077w	ν(C≡C) str., ν(C=C) str.	dc8: ν_3 = 2094(5211); sc3: ν_{14} = 2031(3); dp10: ν_4 = 2048(62); dp6: ν_3 = 2099(1194); sp8: ν_3 = 2071(3542); sp6: ν_3 = 1993(486)
	1953vw			ν(C≡C) str., ν(C=C) str.	sc5: ν_2 = 1916(27); sp6: ν_3 = 1993(486).
	1863m	1874w	1895vw	δ(C=C–H) sciss., ν(C=C) str.	dc10: ν_3 = 1878(568).
			1664s	ν(C=C) str., ν(C–C–H) str.	dc8: ν_4 = 1639(504); sc6: ν_3 = 1669(90); dp10: ν_5 = 1609(1972); dp6: ν_4 = 1634(218).
1494vs	1547s	1506vs	1507vs	δ(C=C–H) sciss., ν(C=C) str., (C–C–H) str.	dc10: ν_4 = 1509(693); sc3: ν_2 = 1483(19); dp10: ν_5 = 1609(1972).
				δ(C=C–H) sciss.	dc10: ν_5 = 1426(92); dc8: ν_5 = 1463(65); sc3: ν_2 = 1483(19); sc5: ν_3 = 1436(75); sc6: ν_4 = 1428(124).
1337vs	1358s	1349m	1333s	ν(C–C) str., δ(C=C–H) sciss., χ(C–C–H) rock.	dc8: ν_6 = 1332(201); sc5: ν_9 = 1310(1); dp10: ν_6 = 1304(115); dp6: ν_5 = 1313(27); sp8: ν_4 = 1318(30).
1262s	1205m	1218m	1208w	δ(C=C–H) sciss. ν(C=C) str.	dc10: ν_6 = 1241(34); dp10: ν_7 = 1187(109).
	1147m			ν(C–C) str., ν(C=C) str., δ(C=C–H) sciss., χ(C–C–H) rock.	dc10: ν_7 = 1129(968); dc8: ν_7 = 1158(1345); dp10: ν_7 = 1187(109).
1077m	1086m	1036w	1083m	ν(C=C) str., χ(C=C–H) rock.	dc10: ν_{29} = 1000(9); dc8: ν_8 = 1027(8); sc3: ν_3 = 1092(46); dp6: ν_6 = 1028(24).
				ν(C–C) str., ν(C=C–H) sciss.	dc8: ν_8 = 1027(8); dp6: ν_6 = 1028(24).
	954vs		987vw	ν(C=C) str., χ(C=C–H) rock.	dc10: ν_{29} = 1000(9); dc8: ν_9 = 938(122)
827v			858w	ν(C–C) str., χ(C=C–H) wag., χ(C–C–H) rock.	dc10: ν_{32} = 847(5); sc5: ν_{14} = 837(4); sc6: ν_{14} = 851(17); dp10: ν_8 = 835(117); dp6: ν_{14} = 850(14).

Band intensities *: very weak (vw), weak (w), mean (m), strong (s), and very strong (vs).**The modes are valence (ν), strain (δ), and out-of-plane (χ).

The correlation of the band intensities in the Raman spectra with the film morphology allows us to conclude that the signal-intensity growth can be attributed to the giant Raman scattering effect. According to the AFM data, the surface is highly developed and the structure height is 280–900 nm (Fig. 5b). They represent agglomerations of Cu atoms coated with a carbon film.

The surfaces of the films formed on the Al substrates were investigated by atomic force microscopy,

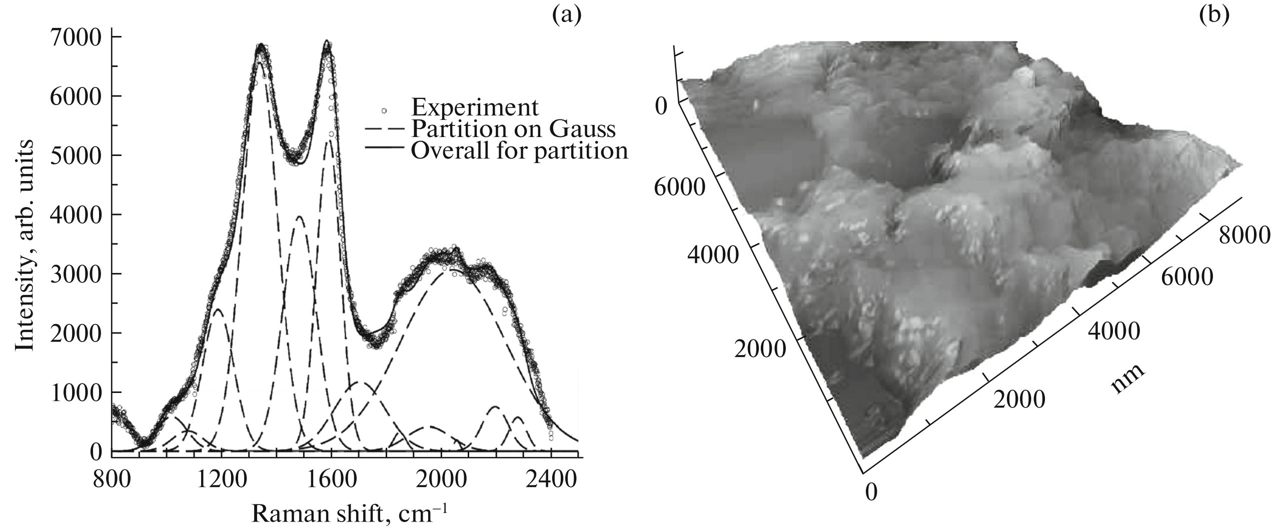

Fig. 5. (a) Raman spectra of the film on the Cu substrate with the decomposition into Gaussian functions and (b) AFM image of the film surface.

which yielded the following results: the surface consists of clusters 170–250 nm in size. Comparing the Raman signal intensity for the films formed on the Al substrate with the signal intensity for the films on other substrates, we can see that, in this case, the intensity has an intermediate value. It is lower for the films on Cu and higher for the films on W and Mo. Since, in the case of Al, the resonance amplification at an excitation wavelength of 633 nm should be lacking, we can speak about another mechanism—the so-called arrester effect, which has a nonresonant character.

For the films on the W and Mo substrates, we observed a weaker developed surface, which can be explained by the formation of compounds of a metal and carbon (the so-called carbide layer). It holds an intermediate position between the metal material of a substrate and carbon film. This layer blocks the formation of a diffuse layer of metal atoms in the carbon matrix. At room temperature, the possible formation of such an intermediate layer is caused by ion stimulation during film synthesis.

4. CONCLUSIONS

This study concerns LCC deposition on various metal substrates (Cu, Mo, W, and Al) under identical experimental conditions. To study their structure and conductivity, we used Raman spectra and tunneling spectroscopy. To determine the possible film structures, we simulated the harmonic oscillations of molecules containing carbon chains with different types of chemical bonds. Comparison of the calculated and experimental Raman spectra allowed us to conclude that the films belonging to the LCC model have chain kinks. The linear fragment lengths were calculated based on the assumptions made previously [5]. The dependence of the film structure on the substrate material was studied.

ACKNOWLEDGMENTS

We thank Prof. M.B. Guseva, associate Prof. V.V. Khvostov, associate Prof. I.K. Gainullina, and R.S. Shutskii for discussion of the results of investigations and analyzing the data obtained.

REFERENCES

1. V. G. Babaev, M. B. Guseva, N. D. Novikov, V. V. Khvostov, and P. Flood, *Polyynes Synthesis, Properties and Application*, Ed. by F. Cataldo (CRC, Boca Raton, FL, 2006).
2. US Patent No. 6.355.350.B1 (2002).
3. V. G. Babaev, M. B. Guseva, N. F. Savchenko, N. D. Novikov, V. V. Khvostov, and P. Flad, J. Surf. Invest.: X-ray, Synchrotr. Neutron Tech. **3**, 16 (2004).
4. V. V. Khvostov, I. P. Ivanenko, O. A. Streletskiy, N. D. Novikov, V. G. Yakunin, and N. F. Savchenko, JETP Lett. **97**, 231 (2013).
5. E. A. Buntov, A. F. Zatsepin, M. B. Guseva, and Yu. S. Ponosov, Carbon **117**, 271 (2017).
6. N. S. Maslova, S. I. Oreshkin, V. I. Panov, and S. V. Savinov, JETP Lett. **67**, 146 (1998).
7. T. K. Zvonareva, V. I. Ivanov-Omskii, V. V. Rozanov, and L. V. Sharonova, Semiconductors **35**, 1398 (2001).
8. A. O. Golubok, O. M. Gorbenko, T. K. Zvonareva, S. A. Maslov, V. V. Rozanov, S. G. Yastrebov, and V. I. Ivanov-Omskii, Semiconductors **34**, 217 (2000).
9. N. S. Maslova, Yu. N. Moiseev, S. V. Savinov, and R. G. Yusupov, JETP Lett. **58**, 528 (1993).

10. K. S. Nakayama, M. G. Alemany, T. Sugano, K. Ohmori, H. Kwak, J. R. Chelikowsky, and J. H. Weaver, Phys. Rev. B **73**, 035330 (2006).
11. Z. Klusek, P. Kowalczyk, and P. Byszewski, Vacuum **63**, 145 (2001).
12. J. G. Simmons, J. Appl. Phys. **34**, 1793 (1963).
13. J. G. Simmons, J. Appl. Phys. **34**, 238 (1963).
14. Advanced Technology Center RU. http://www.nanoscopy.net/en/.
15. W. A. Chalifoux and R. R. Tykwinski, Nat. Chem. **2**, 967 (2010).
16. A. Milani, M. Tommasini, V. Russo, A. L. Bassi, A. Lucotti, F. Cataldo, and C. S. Casari, Beilstein J. Nanotechnol. **6**, 480 (2015).
17. J. G. Korobova and D. I. Bazhanov, JETP Lett. **93**, 730 (2011).
18. V. M. Melnichenko, A. M. Sladkov, and J. N. Nikulin, Russ. Chem. Rev. **51**, 421 (1982).
19. C. Casiraghi, F. Piazza, A. C. Ferrari, D. Grambole, and J. Robertson, Diamond Relat. Mater. **14**, 1098 (2005).
20. M. J. Frisch, G. W. Trucks, H. B. Schlegel, et al., *Gaussian'03, Revision B.03* (Gaussian Inc., Pittsburgh, 2003).
21. S. V. Krasnoshchekov and N. F. Stepanov, J. Phys. Chem. **82**, 690 (2008).
22. S. V. Krasnoshchekov, E. V. Isayeva, and N. F. Stepanov, J. Phys. Chem. A **116**, 3691 (2012).
23. S. V. Krasnoshchekov, N. C. Craig, P. Boopalachandran, J. Laane, and N. F. Stepanov, J. Phys. Chem. **119**, 10706 (2015).
24. Y. N. Panchenko, S. V. Krasnoshchiokov, and C. W. Bock, J. Comput. Chem. **9**, 443 (1988).
25. A. D. Boese, W. Klopper, and J. M. L. Martin, Int. J. Quant. Chem. **104**, 830 (2005).
26. A. C. Ferrari and J. Robertson, Phys. Rev. B **64**, 075414 (2001).
27. A. Milani, M. Tommasini, V. Russo, A. li Bassi, A. Lucotti, F. Cataldo, and S. Carlo, Beiltein J. Nanotechnol. **6**, 480 (2015).
28. A. C. Ferrari and J. Robertson, Phys. Rev. B **61**, 14095 (2000).
29. A. N. Obraszov, A. P. Volkov and I. Yu. Pavlovsky, JETP Lett. **68**, 56 (1998).
30. C. S. Casari, A. li Bassi, A. Baserga, L. Ravagnan, P. Piseri, C. Lenardi, M. Tommasini, A. Milani, D. Fazzi, C. E. Bottani, and P. Milani, Phys. Rev. B **77**, 195444 (2008).
31. M. Rybachuka and J. M. Bellb, Carbon **47**, 2481 (2009).
32. E. Cinquanta, L. Ravagnan, I. Eligio Castelli, F. Cataldo, N. Manini, G. Onida, and P. Milani, J. Chem. Phys. **135**, 194501 (2011).
33. P. K. Chu and L. Li, Mater. Chem. Phys. **96**, 253 (2006).
34. J. A. Lenz, C. A. Perottoni, N. M. Balzaretti, and J. A. H. da Jornada, J. Appl. Phys. **89**, 8284 (2001).
35. A. C. Ferrari and J. Robertson, Phys. Rev. B **64**, 075414 (2001).
36. Sh. Li, G. Ji, Zh. Huang, F. Zhang, and Y. Du, Carbon **45**, 2946 (2007).
37. H. Kuzmany and P. Knoll, Springer Ser. Solid State Sci. **63**, 114 (1985).
38. M. Chhowalla, A. C. Ferrari, J. Roberston, and G. A. J. Amaratunga, Appl. Phys. Lett. **76**, 1419 (2000).
39. F. Cataldo and D. Capitani, Mater. Chem. Phys. **59**, 225 (1999).
40. J. A. Lenz, C. A. Perottoni, N. M. Balzaretti, and J. A. H. da Jornada, J. Appl. Phys. **89**, 8284 (2001).
41. L. Kavan, J. Hlavaty, J. Kastner, and H. Kuzmany, Carbon **33**, 1321 (1995).
42. A. V. Baranov, A. N. Bekhterev, Y. S. Bobovich, and V. I. Petrov, Opt. Spectrosc. (USSR) **62**, 612 (1987).

Translated by E. Bondareva